JACS
JOURNAL OF THE AMERICAN CHEMICAL SOCIETY
pubs.acs.org/JACS
Article

Direct Probes of π-Delocalization in Prototypical Resonance-Stabilized Radicals: Hyperfine-Resolved Microwave Spectroscopy of Isotopic Propargyl and Cyanomethyl

P. Bryan Changala,* Peter R. Franke, John F. Stanton, G. Barney Ellison, and Michael C. McCarthy*

Cite This: J. Am. Chem. Soc. 2024, 146, 1512–1521
Read Online
ACCESS | Metrics & More | Article Recommendations | Supporting Information

ABSTRACT: Delocalization of the unpaired electron in π-conjugated radicals has profound implications for their chemistry, but direct and quantitative characterization of this electronic structure in isolated molecules remains challenging. We apply hyperfine-resolved microwave rotational spectroscopy to rigorously probe π-delocalization in propargyl, CH_2CCH, a prototypical resonance-stabilized radical and key reactive intermediate. Using the spectroscopic constants derived from the high-resolution cavity Fourier transform microwave measurements of an exhaustive set of ^{13}C- and ^{2}H-substituted isotopologues, together with high-level ab initio calculations of zero-point vibrational effects, we derive its precise semiexperimental equilibrium geometry and quantitatively characterize the spatial distribution of its unpaired electron. Our results highlight the importance of considering both spin-polarization and orbital-following contributions when interpreting the isotropic hyperfine coupling constants of π radicals. These physical insights are strengthened by a parallel analysis of the isoelectronic species cyanomethyl, CH_2CN, using new ^{13}C measurements also reported in this work. A detailed comparison of the structure and electronic properties of propargyl, cyanomethyl, and other closely related species allows us to correlate trends in their chemical bonding and electronic structure with critical changes in their reactivity and thermochemistry.

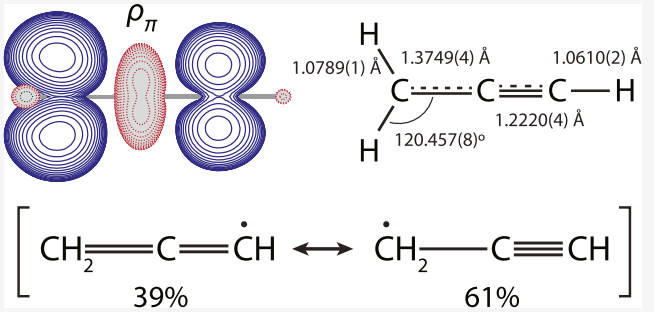

INTRODUCTION

Propargyl, CH_2CCH, is one of the simplest conjugated π radicals. Like other resonance-stabilized radicals, it plays a crucial role in hydrocarbon growth in combustion, atmospheric, and astronomical environments.[1−3] Its barrierless and exothermic self-reaction produces benzene and phenyl radical, the first steps in ring formation,[4−7] and it contributes to the initiation and propagation of radical chain reactions proposed as efficient growth mechanisms for polycyclic aromatic hydrocarbons (PAHs) and, ultimately, soot and dust particles.[8] Characterizing the relationship between the structure and reactivity of propargyl and similar radicals provides important insights into the complex chemical pathways that they drive.

Spectroscopic observations of propargyl in the gas[9−14] and condensed[15−20] phases have established that it exhibits a planar C_{2v} equilibrium geometry, consistent with a π-delocalized resonance structure of intermediate ethynyl methyl and allenyl character, $H_2\dot{C}-C{\equiv}CH \leftrightarrow H_2C{=}C{=}\dot{C}H$. The most direct spectroscopic probes of this π-electron distribution are electron spin resonance (ESR)[15,16,21] and hyperfine-resolved microwave[12] measurements of nuclear-electron magnetic dipole interactions, which are sensitive to the unpaired electron spin density and distribution around each nucleus of nonzero spin, I. Because ^{12}C has $I = 0$, prior ESR and microwave studies of the parent isotopic species have reported the hyperfine coupling constants (HCCs) only for the hydrogen spins, and we thus lack a complete description of the π-electron system along the carbon backbone. Moreover, with the exception of one infrared study of H_2CCCD,[22] there are no high-resolution gas-phase measurements of partially or fully deuterated propargyl, which would enable the derivation of its molecular structure and provide a valuable complementary picture of its π conjugation.

In this paper, we present a comprehensive analysis of the hyperfine-resolved microwave spectra of an extensive set of ^{13}C- and ^{2}H-substituted propargyl isotopologues. The measured ground-state rotational constants, corrected by high-level ab initio zero-point vibrational calculations, are used to derive a precise semiexperimental equilibrium geometry, while the ^{13}C, ^{1}H, and ^{2}H HCCs provide a complete description of the spatial distribution of the unpaired electron. We show that the ^{13}C isotropic HCCs, $a_F(^{13}C)$, have

Received: October 10, 2023
Revised: December 5, 2023
Accepted: December 6, 2023
Published: January 3, 2024

https://doi.org/10.1021/jacs.3c11220
J. Am. Chem. Soc. 2024, 146, 1512−1521

significant contributions from s/p rehybridization of the singly occupied π orbital induced by out-of-plane zero-point vibrational motion[23]—a one-electron effect of comparable magnitude to the more commonly considered electron correlation (spin-polarization) contributions to $a_F(^{13}C)$.

The derived equilibrium structure and electronic properties of CH_2CCH are used to evaluate the relative weight of the nominal ethynyl methyl and allenyl resonance structures in its ground electronic state, which has important implications for its patterns of C−C bond formation. This analysis is deepened by a comparison to several closely related chemical species, in particular, the isoelectronic cyanomethyl radical, CH_2CN, the ^{13}C spectra of which are also reported here for the first time. Through a parallel analysis of its geometry and hyperfine structure, we quantify how the radical electron is influenced by changes in the electronegativity of the π system constituents and connect these differences to trends in their reactivity and thermochemistry.

EXPERIMENTAL SECTION

Propargyl radicals were produced in a pulsed discharge-supersonic expansion source coupled to a cavity-enhanced Fourier transform microwave (FTMW) spectrometer operating from 6 to 24 GHz.[24,25] The discharge conditions were similar to that of the original FTMW experiments by Tanaka et al.[12] A dilute (0.1−0.2%) mix of an organic precursor in neon was expanded at a backing pressure of 2500 Torr in 400−600 μs gas pulses at 5 Hz. A 20−30 mA discharge was struck during the gas pulse between two copper ring electrodes spaced by 1 cm and held at a 1 kV potential difference. The gas mixture was expanded into vacuum along the axis of a confocal microwave cavity formed by two large spherical mirrors, rapidly cooling to a rotational temperature of approximately 2 K.[26] The molecules in the cavity were excited with a 1 μs pulse of resonant radiation, and the subsequent free induction decay was detected by a sensitive microwave receiver, digitally recorded, and Fourier transformed, resulting in a double-peaked (Doppler-splitting) line shape centered about the rest frequency, which is determined to an accuracy of 2 kHz. Three perpendicular pairs of Helmholtz coils were placed around the vacuum chamber to null the Earth's magnetic field, which otherwise causes large Zeeman splittings of the radical microwave transitions (well in excess of the ∼5 kHz fwhm line width of each Doppler-doublet component).

The small permanent dipole moment of propargyl (μ = 0.15 D[27]) required the use of isotopically enriched precursors to generate detectable amounts of substituted propargyl radicals. $H_2^{13}CCCH$ and $H_2CC^{13}CH$ were produced from propene-1-^{13}C, while $H_2C^{13}CCH$ was produced from propene-2-^{13}C (both supplied by CDN Isotopes). The deuterated species H_2CCCD, HDCCCH, and HDCCCD were produced from 1,3-butadiene-2,3-d_2 (CDN Isotopes); D_2CCCH was produced from 1,3-butadiene-1,1,4,4-d_4 (CDN Isotopes); and D_2CCCD was obtained from 1,3-butadiene-d_6 (Sigma-Aldrich). At our source conditions, propene and 1,3-butadiene generated only 10% of the number of propargyl radicals relative to propargyl chloride,[12] which is the most efficient discharge precursor we have measured, but for which isotopic samples are prohibitively expensive. The yield from benzene was only 1% relative to that from propargyl chloride, consistent with the large number of other products produced in benzene discharges.[28]

Cyanomethyl radicals were produced with discharge conditions similar to those of propargyl using pure samples of ^{13}C-labeled acetonitrile ($^{13}CH_3CN$ and $CH_3^{13}CN$ for $^{13}CH_2CN$ and $CH_2^{13}CN$, respectively, both supplied by Sigma-Aldrich). The ^{13}C species were readily observed and assigned using predictions based on the well-determined rotation, fine, and hyperfine parameters of the parent isotopologue.[29−35]

THEORY

Electronic structure calculations of propargyl were carried out with the CFOUR program package.[36,37] The equilibrium geometry was optimized with all-electron coupled cluster calculations including singles, doubles, and perturbative triples excitations [CCSD(T)] with a restricted open-shell Hartree−Fock (ROHF) reference wave function[38] and the Dunning correlation-consistent triple-, quadruple-, and pentuple-ζ basis sets, cc-pCV(T,Q,5)Z.[39] The zero-point contributions to the rotational constants were determined with second-order vibrational perturbation theory[40] (VPT2) using cubic force constants calculated by finite differences at the ROHF-CCSD(T)/cc-pCVQZ level of theory. The electronic g-tensor contribution[41] was calculated with an unrestricted Hartree−Fock (UHF) reference wave function at the CCSD(T)/cc-pCVTZ level of theory. A variety of additional higher-order corrections were calculated to reach a theoretical prediction of sub-mÅ target accuracy.[42] The CCSD(T) complete basis set (CBS) limit was approximated by extrapolation of all-electron CCSD(T)/cc-pCVXZ structural parameters with X = T, Q, 5. Scalar relativistic corrections were calculated at the CCSD(T)/cc-pCVTZ level; quadruple excitation valence correlation effects by the difference of frozen-core CCSD(T) and CCSDT(Q) geometries with the cc-pVDZ basis set; and diagonal Born−Oppenheimer corrections (DBOC) by analytic DBOC calculations at the HF level with the cc-pCVTZ basis set.

The isotropic HCCs were evaluated by analytic coupled cluster gradient methods implemented in CFOUR. Vibrational corrections to these HCCs were calculated with reduced-dimension variational vibrational calculations using the NITROGEN package[43] and with full-dimensional VPT, implemented with Mathematica,[44] using CFOUR cubic force fields. The force fields of both propargyl and cyanomethyl radicals were first determined at the frozen-core equation-of-motion ionization-potential (EOM-IP) CCSDT/ANO1 level of theory based on finite differences of analytic gradients.[45−47] It was anticipated that this approach would provide a reliable description of the vibrational structure of both radicals, as it uses a well-behaved closed-shell anion reference wave function, it includes adequate electron correlation, and the ANO1 basis set tends to describe systems with multiply bonded carbons more accurately than Dunning basis sets of similar size.[48] Next, from the EOM-IP-CCSDT/ANO1 optimized structures, isotropic HCCs were evaluated at the all-electron UHF-CCSD/cc-pCVQZ level of theory at ±0.05 unit displacements in the EOM-IP-CCSDT/ANO1 dimensionless normal coordinates.[39,49,50] First and diagonal second derivatives of the isotropic HCCs were determined by finite differences and used to obtain ground-state values via the general expression for a vibrationally averaged property.[51,52] VPT vibrational averages were based on the normal isotopologues of propargyl and cyanomethyl.

RESULTS AND DISCUSSION

Rotational and Hyperfine Parameters. Propargyl and cyanomethyl are both near-prolate asymmetric tops with $^2B_1$ ground electronic states. The molecular Hamiltonian includes fine and hyperfine interactions described by

$$H = H_{rot} + H_{spin-rot} + H_{hfs}$$

https://doi.org/10.1021/jacs.3c11220
J. Am. Chem. Soc. 2024, 146, 1512−1521

Table 1. Spectroscopic Constants of Propargyl[a]

parameter	H_2CCCH[b]	H_2CCCD	D_2CCCH	D_2CCCD	DHCCCH	HDCCCD	$H_2CC^{13}CH$	$H_2C^{13}CCH$	$H_2^{13}CCCH$
A	[288055]	[287998.8][c]	[144460.3][c]	[144444.8][c]	[198233.2][c]	[198035.4][c]	[288053.3][c]	[288044.7][c]	[288048.7][c]
$(B + C)/2$	9365.2790(48)	8499.6329(3)	8252.7825(4)	7523.9975(3)	8758.4386(4)	7969.0018(6)	9081.8719(4)	9363.9651(2)	9092.1819(3)
$B - C$	316.7970(72)	[260.997][c]	[484.497][c]	[402.896][c]	[400.297][c]	[331.796][c]	[297.997][c]	[316.596][c]	[298.597][c]
ϵ_{aa}	−529.386(60)	[−529.283][d]	[−265.488][d]	[−265.460][d]	[−364.312][d]	[−363.948][d]	[−529.383][d]	[−529.367][d]	[−529.374][d]
ϵ_{bb}	−11.524(30)	−10.480(5)	−10.272(4)	−9.367(5)	−10.835(5)	−9.958(12)	−11.175(4)	−11.532(3)	−11.191(5)
ϵ_{cc}	−0.520(30)	[−0.473][d]	[−0.452][d]	[−0.414][d]	[−0.483][d]	[−0.441][d]	[−0.505][d]	[−0.520][d]	[−0.505][d]
a_F (acet.)	−36.323(24)	−5.677(10)	−36.402(32)	−5.665(4)	−36.337(46)	−5.715(32)	[−36.323][e]	[−36.323][e]	[−36.323][e]
T_{aa}	17.400(24)	2.722(7)	17.418(5)	2.728(6)	17.370(19)	2.749(30)	[17.400][e]	[17.400][e]	[17.400][e]
T_{bb}	−17.220(37)	[−2.643][e]	[−17.220][e]	[−2.643][e]	[−17.220][e]	[−2.643][e]	[−17.220][e]	[−17.220][e]	[−17.220][e]
χ_{aa}		0.213(5)		0.202(4)		0.210(11)			
χ_{bb}		[−0.114][f]		[−0.114][f]		[−0.114][f]			
a_F (meth.)	−54.21(11)	−54.296(73)	−8.350(3)	−8.356(12)	−8.319(2)	−8.331(17)	[−54.210][e]	[−54.210][e]	[−54.210][e]
T_{aa}	−14.121(19)	−14.156(7)	−2.210(6)	−2.219(6)	−1.956(5)	−2.166(29)	[−14.121][e]	[−14.121][e]	[−14.121][e]
T_{bb}	[12.88]	[12.88][e]	[1.977][e]	[1.977][e]	[1.977][e]	[1.977][e]	[12.88][e]	[12.88][e]	[12.88][e]
χ_{aa}			0.019(3)	0.016(5)	−0.010(3)	−0.031(22)			
χ_{bb}			[0.129][f]	[0.129][f]	[0.129][f]	[0.129][f]			
a_F'					−54.416(101)	−55.037(276)			
T_{aa}'					−15.705(15)	−15.676(10)			
T_{bb}'					[12.88][e]	[12.88][e]			
$a_F(^{13}C)$							51.334(46)	−65.303(32)	78.100(50)
T_{aa}							−37.004(6)	18.682(6)	−58.993(7)
T_{bb}							[−31.489][f]	[1.186][f]	[−60.439][f]
(N, χ_{red})[g]		(10, 0.6)	(11,0.6)	(14, 0.4)	(15, 0.3)	(12, 0.4)	(9, 3.1)	(15, 1.5)	(10, 2.6)

[a]All values are in MHz with 1σ uncertainties in parentheses. Values in square brackets are held fixed. Centrifugal distortion constants (not shown) are fixed for all isotopologues to those used by Tanaka et al.[12] for the parent isotopologue scaled by the calculated isotopic ratios. [b]Values from Tanaka et al.[12] [c]Fixed to normal isotopologue value plus calculated isotope shift. [d]Fixed to normal isotopologue value scaled by calculated A_0 or C_0 ratio. [e]Fixed to normal isotopologue value scaled by D/H g-factor ratio of 0.1535, as necessary. [f]Fixed to CCSD(T)/cc-pCVTZ calculated value. [g]The number of hyperfine transitions observed and the reduced χ value of the fit, assuming a measurement uncertainty of 2 kHz.

https://doi.org/10.1021/jacs.3c11220
J. Am. Chem. Soc. 2024, 146, 1512−1521

where H_{rot} is the standard A-reduced (in the I^r representation) rotational Hamiltonian with quartic centrifugal distortion[53] and

$$H_{spin-rot} = \epsilon_{aa}N_aS_a + \epsilon_{bb}N_bS_b + \epsilon_{cc}N_cS_c$$

accounts for spin-rotation interactions.[54] The hyperfine term, H_{hfs}, contains an isotropic Fermi contact interaction (a_F) and anisotropic dipole−dipole (T_{aa}, T_{bb}, and T_{cc}) coupling for each nucleus i with $I_i > 0$

$$H_{hfs,i} = a_F\mathbf{S}\cdot\mathbf{I_i} + T_{aa}S_aI_{ia} + T_{bb}S_bI_{ib} + T_{cc}S_cI_{ic}$$

where $T_{aa} + T_{bb} + T_{cc} = 0$. Nuclear electric quadrupole coupling, parametrized by χ_{aa} and χ_{bb}, is also added for deuterium and ^{14}N nuclei ($I = 1$).[55]

Only the $N_{K_a,K_c} = 1_{01} - 0_{00}$ transition for each isotopologue is within our instrument bandwidth. This transition is split into several fine and hyperfine components, which are sufficient to determine only a subset of the spectroscopic constants, including $(B + C)/2$, ϵ_{bb}, a_F, and T_{aa} for each dipolar nucleus ($I \neq 0$), as well as χ_{aa} for each quadrupolar deuterium nucleus ($I = 1$). The best-fit values were optimized with the SPFIT program[56] and are summarized in Tables 1 and 2. The undetermined constants were fixed to (appropriately scaled[57]) values of the normal isotopologues of propargyl[12] and cyanomethyl,[35] or to calculated values as described in the table notes. The complete measured line lists and fit files are available in the Supporting Information.

Semiexperimental Equilibrium Geometry. Although the microwave data set of propargyl is insufficient to determine all three rotational constants independently, the large number of isotopologues does permit a structure determination using the measured values of just $(B + C)/2$ (and $B - C$ of the main isotopologue). After correcting for zero-point vibration and electronic contributions to the rotational constants using the theoretical calculations summarized in Table 3, we performed a least-squares optimization of the five independent structural parameters (two CC bond lengths, two CH bond lengths, and one CCH bond angle assuming planar C_{2v} symmetry) to derive a semiexperimental equilibrium geometry, r_e^{SE}. The best-fit structure, shown in Figure 1, reproduces the measured values of $(B + C)/2$ for the nine isotopic species with an rms residual of 27 kHz. The best theoretical r_e estimate (Table 4) agrees with the semiexperimental equilibrium geometry to sub-mÅ accuracy.

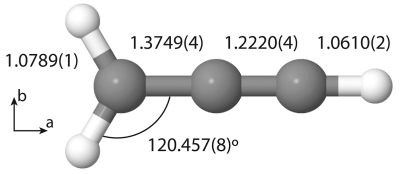

Figure 1. Semiexperimental equilibrium structure of propargyl. Bond lengths are shown in Å. The value in parentheses is the 2-σ uncertainty (in units of the last digit). The principal a and b axes are labeled.

An equal balance between the nominal ethynyl methyl and allenyl resonance structures

$$\dot{C}H_2{-}C{\equiv}CH \leftrightarrow CH_2{=}C{=}\dot{C}H$$

would imply effective CC bond orders of 1.5 and 2.5 for the $CH_2{-}CCH$ and $CH_2C{-}CH$ bonds, respectively.[16,19,21] This qualitative representation is borne out by a comparison of the equilibrium structure of propargyl to several closely related species, the CC bond lengths of which are collected in Table 5. The $CH_2{-}CCH$ bond in propargyl is 0.083 Å shorter than the single bond in either propyne or acetonitrile, while it is only 0.043 Å longer than the double bond in propene or ethylene.

Table 2. Spectroscopic Constants of ^{13}C Cyanomethyl[a]

parameter[b]	$H_2^{13}CCN$	$H_2C^{13}CN$
A	[284994.4][c]	[284994.4][c]
$(B + C)/2$	9748.1774(2)	10059.1827(2)
$B - C$	[347.9330][c]	[369.5179][c]
ϵ_{aa}	[−661.5305][c]	[−661.5305][c]
ϵ_{bb}	[−23.3460][c]	[−24.10667][c]
ϵ_{cc}	[−1.97625][c]	[−2.0383][c]
$a_F(^{13}C)$	89.020(10)	−63.724(5)
T_{aa}	−66.136(3)	18.410(3)
T_{bb}	[−67.62][d]	[0.585][d]
(N, χ_{red})[e]	(43, 2.6)	(40, 2.5)

[a]All values are in MHz with 1σ uncertainties in parentheses. Values in brackets are held fixed. [b]The quartic centrifugal distortion constants and hyperfine constants for ^{14}N and H nuclei (not shown) are assumed equal to their values in the normal isotopologue reported in ref 35. [c]Predicted by scaling the experimental values of the normal isotopologue[35] with the isotope shifts calculated using the equilibrium geometry in ref 31. [d]Fixed to the equilibrium all-electron UHF-CCSD(T)/cc-pCV5Z value. [e]The number of hyperfine transitions observed and the reduced χ value of the fit, assuming a measurement uncertainty of 2 kHz.

Table 3. Vibrational and Electronic Corrections to Propargyl Rotational Constants[a]

parameter[b]	H_2CCCH	H_2CCCD	D_2CCCH	D_2CCCD	DHCCCH	HDCCCD	$H_2CC^{13}CH$	$H_2C^{13}CCH$	$H_2^{13}CCCH$
A_e	290279.8	290279.8	145251.5	145251.5	199258.6	199071.9	290279.8	290279.8	290279.8
B_e	9527.1	8629.5	8494.8	7722.2	8960.2	8133.1	9235.0	9525.8	9244.3
C_e	9224.4	8380.4	8025.5	7332.4	8574.6	7813.8	8950.2	9223.1	8959.0
$A_e - A_0$	2102.9	2159.2	669.4	684.9	903.6	914.6	2104.6	2113.2	2109.3
$B_e - B_0$	11.4	7.0	6.9	3.6	9.1	5.3	11.8	11.5	10.6
$C_e - C_0$	24.7	18.0	21.0	15.6	23.0	16.9	24.3	24.8	23.2
ΔA_{el}	−177.290	−177.290	−44.410	−44.410	−83.510	−83.360	−177.290	−177.290	−177.290
ΔB_{el}	−0.092	−0.076	−0.074	−0.061	−0.082	−0.067	−0.087	−0.092	−0.087
ΔC_{el}	0.061	0.050	0.046	0.038	0.052	0.044	0.057	0.061	0.057

[a]All values are given in MHz. [b]The equilibrium (A_e, B_e, and C_e) constants are calculated at the ROHF-CCSD(T)/cc-pCVQZ level of theory. The zero-point corrections ($A_e - A_0$, $B_e - B_0$, and $C_e - C_0$) are calculated with VPT and cubic force constants with the same electronic structure method. The electronic (rotational g tensor) corrections (ΔA_{el}, ΔB_{el}, and ΔC_{el}) are calculated at the UHF-CCSD(T)/cc-pCVTZ level of theory.

https://doi.org/10.1021/jacs.3c11220
J. Am. Chem. Soc. 2024, 146, 1512−1521

Table 4. Theoretical (r_e) and Semiexperimental (r_e^{SE}) Equilibrium Structures of Propargyl[a]

parameter	ae-CCSD(T)/CBS	$\Delta_{rel} \times 10^4$	$\Delta_{T(Q)} \times 10^4$	$\Delta_{DBOC} \times 10^4$	best r_e	r_e^{SE}[b]
$r(H_2CCC-H)$	1.06136	−1.5	−0.9	+1.4	1.06126	1.0610(2)
$r(H_2-CCCH)$	1.07810	−1.3	+1.7	+1.3	1.07827	1.0789(1)
$r(H_2CC\equiv CH)$	1.22174	−2.6	+9.6	−1.2	1.22232	1.2220(4)
$r(H_2C-CCH)$	1.37421	−2.6	+1.6	+0.6	1.37417	1.3749(4)
∠(HCC)	120.482[c]	−40	+60	−261	120.458	120.457(8)

[a]All values are in Å or degrees. [b]The value in parentheses is the 2-σ uncertainty in units of the last digit. [c]The ∠(HCC) angle exhibited nonmonotonic changes with increasing basis set size. In lieu of an exponential extrapolation, its CBS limit was estimated by the optimized CCSD(T)/cc-pCV5Z value.

Table 5. Equilibrium CC Bond Lengths in Small Hydrocarbon and Nitrile Molecules and Radicals

molecule	r_{C-C}	$r_{C=C}$	$r_{C\equiv C}$	reference
CH_3CCH	1.45884(6)		1.20460(7)	58
CH_2CCH_2		1.307(1)		59
CH_3CN	1.4586(3)			60
C_2H_2			1.202866(72)	61
C_2H_4		1.3305(10)		62
CH_2CHCH_3	1.49530(25)	1.33148(26)		63
$\cdot CH_2CN$	1.3903(5)			31
$\cdot CH_2CCH$	1.3747(5)		1.2222(5)	this work

Conversely, the CH_2C-CH bond in propargyl is 0.017−0.019 Å longer than the C≡C triple bond in propyne or acetylene. These significant bond length differences are evidence of π-delocalization of the unpaired electron along the carbon backbone.

It is also insightful to compare the structure of propargyl with the isoelectronic cyanomethyl radical, CH_2CN. While the CC single bonds in the parent molecules CH_3-CCH and CH_3-CN differ by less than 0.001 Å, the CH_2-CN bond length is 0.016 Å longer than the CH_2-CCH bond length, which indicates that the unpaired electron is more highly localized at the CH_2 center in CH_2CN than in CH_2CCH. This outcome is what would be expected based on the relative electronegativities of the ≡N vs ≡CH fragments. The hyperfine coupling parameters of CH_2CCH and CH_2CN, discussed below, provide complementary and additional direct evidence for this change in the electronic structure.

Hyperfine Structure. HCCs provide direct measurements of the electronic wave function of open-shell molecules. The isotropic, or Fermi contact, coupling constant, a_F, is proportional to the electron spin density at each nucleus

$$a_F = 800.237\ \text{MHz} \times g\rho(0) \quad (1)$$

where $\rho(0)$ is the total electron spin density at the given nucleus (in a.u.), and g is its nuclear g-factor.[64] The anisotropic HCC T_{aa} provides additional information about the orientation of the unpaired spin density about the a symmetry axis[65]

$$T_{aa} = 95.521\ \text{MHz} \times g \times \left\langle \frac{3\cos^2\theta - 1}{r^3} \right\rangle_{\text{unpaired}} \quad (2)$$

where r (in a.u.) is the distance from the given nucleus and θ the angle with respect to the a axis.

In the original microwave study of propargyl by Tanaka et al.,[12] the proton a_F constants of the parent isotopologue were used to infer the spin population of the neighboring C p_π orbitals indirectly with the well-known empirical relation describing this spin-polarization effect,[66] $a_F(H) \approx Q\rho_\pi$, where $Q \approx -64$ MHz and ρ_π is the total spin population in the atomic p_π orbital. Using this relation, they estimated $\rho_\pi \approx 0.84$ and 0.56 for the methylenic (CH_2) and acetylenic (CH) carbon atoms, respectively. Assuming the total π spin population of the three C atoms is unity, this implies that $\rho_\pi \approx -0.40$ for the central C atom. The analysis of the ^{13}C isotopic species in this work in principle provides a direct characterization of the π spin populations, but a meaningful analysis requires an accurate accounting of the contributions to the measurable isotropic and anisotropic ^{13}C HCCs.

We first focus on the isotropic constants (a_F) and two effects—spin polarization and orbital following—that contribute to the spin densities at the atomic nuclei. For planar π radicals like propargyl and cyanomethyl, the singly occupied molecular orbital has a node in the plane of the molecule. Thus, an ROHF wave function has exactly zero spin density at the atomic nuclei. A correlated electronic wave function accounts properly for interactions between the unpaired π electron and paired σ electrons, which increase the spin density in the shared atoms' s orbitals and decrease the spin density at adjacent atoms.[66] In methyl radical, for example, where $\rho_\pi \sim 1$, the spin density is about +0.070 a.u. at the C nucleus (at the planar equilibrium geometry) and −0.014 a.u. for each of the adjacent H nuclei.[67]

A second important source of nonzero spin density in π radicals is orbital following upon vibrational deformation.[23] When the molecule is bent out of plane, the p_π orbitals mix with the 2s orbitals. Even a small amount of s character leads to a large increase in the net spin density owing to the considerable 2s orbital density at the atomic nucleus ($|\psi_{2s}(0)|^2 \approx 3.36$ a.u. for C[68]). The extent of orbital mixing is proportional to the amplitude of out-of-plane deformations, so this effect is most important for C atoms bonded to H atoms, the small masses of which result in significant out-of-plane amplitude, even in the zero-point vibrational level. For CH_3, the vibrationally averaged contribution to the C nuclear spin density is about +0.026 a.u., a considerable fraction (40%) of the spin-polarization contribution. Because the orbital following is predominately a one-electron effect, it can be treated accurately with relatively simple quantum chemical methods. However, it is also essential to use an accurate

https://doi.org/10.1021/jacs.3c11220
J. Am. Chem. Soc. 2024, 146, 1512−1521

anharmonic zero-point vibrational wave function to calculate the vibrationally averaged value,[69,70] which may require more sophisticated electronic structure methods than the electronic property surface itself.

A simple one-dimensional picture of the out-of-plane deformations of CH_3 and the $-CH_2$ group of propargyl is shown in Figure 2. The top panel shows the spin density at the ^{13}C nucleus as a function of the out-of-plane angle. At the planar equilibrium geometry (θ = 90°), there is a small, positive spin density of 0.050−0.070 a.u. from $\pi-\sigma$ spin-polarization. As the molecule is bent out of plane, the spin density quickly increases as the π orbital rehybridizes. The corresponding vibrational potential energy curves are plotted in the bottom panel along with the zero-point vibrational probability densities, $|\Psi(\theta)|^2$. The spin density in $^{13}CH_3$ increases from its equilibrium value of 0.065 a.u. to a vibrationally averaged value of 0.087 a.u., an increase of 34%, in good agreement (considering the one-dimensional approximation) with the experimentally derived vibrational contribution of 40%.[67]

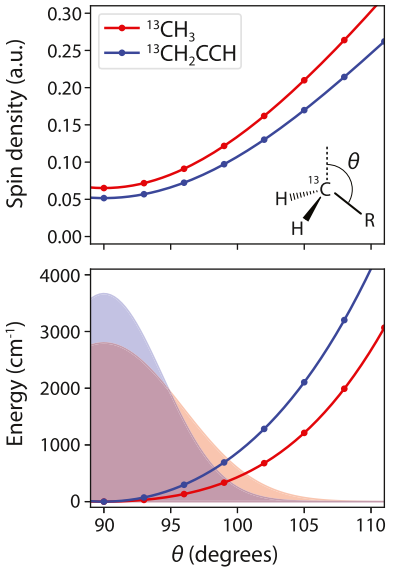

Figure 2. Out-of-plane deformation of methyl and propargyl. The top panel shows the unpaired electron spin density at the carbon nucleus versus the out-of-plane pyramidal bending angle, θ. The bottom panel shows the potential energy curves and corresponding one-dimensional probability densities, $|\Psi(\theta)|^2$. The calculations were performed at the UHF-CCSD(T)/cc-pCVQZ level of theory, holding all structural parameters except θ to their equilibrium values.

The methylenic $-CH_2$ fragment of propargyl behaves similarly to methyl. Its equilibrium and vibrationally averaged C spin densities are 0.052 and 0.062 a.u., respectively, an increase of 20%. Although not as large as methyl, the vibrational correction in propargyl is still substantial. The absolute orbital-following contribution to the spin density is actually quite similar to that of methyl for a given θ. The smaller net correction reflects instead the more contracted zero-point motion of propargyl, which is due to both its tighter bending force constant and the larger effective mass of its out-of-plane vibrational mode.

The acetylenic −CH fragment of propargyl is also susceptible to orbital-following effects, as illustrated in Figure 3, which shows two-dimensional spin density and potential energy contour plots as a function of the out-of-plane (θ) and in-plane (ϕ) bending angles of the hydrogen atom. Like the $-CH_2$ fragment, out-of-plane deformations have a large effect on the C spin density, acquiring a significant s character as the geometry approaches that of an allenyl configuration. Deformations within the plane of the molecule have little effect on the hybridization. The C spin density increases from 0.025 a.u. at the equilibrium geometry to 0.034 a.u. averaged over the two-dimensional vibrational zero-point wave function. This 36% increase is comparable to that observed in CH_3 and even larger than the fractional change of the $-CH_2$ fragment in propargyl.

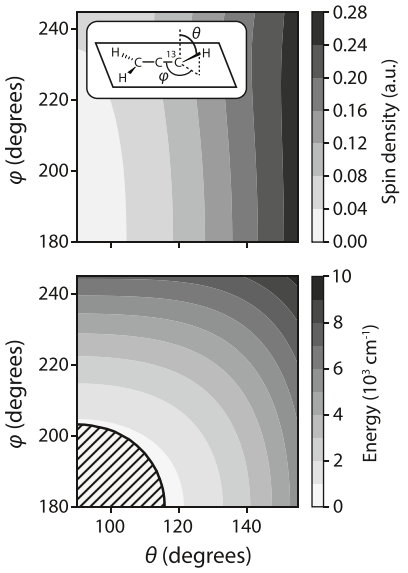

Figure 3. Bending deformation of the acetylenic hydrogen in propargyl. The top panel shows a map of the unpaired spin density at the terminal acetylenic C nucleus versus the out-of-plane (θ) and in-plane (ϕ) bending angles, defined schematically in the inset. The bottom panel shows the corresponding two-dimensional potential energy surface. The hatched region fills the 95% boundary of the zero-point vibrational probability density, $|\Psi(\theta, \phi)|^2$.

Reduced-dimension models capture the qualitative orbital-following effects at play, but a quantitative comparison with the experiment requires accurate full-dimensional vibrational averaging. Tables 6 and 7 summarize our best theoretical estimates for the equilibrium spin densities and ground-state VPT vibrational corrections of propargyl and cyanomethyl, calculated as described in the Theory section above. The tables also include the experimental spin densities derived from the measured isotropic hyperfine constants, a_F, which are

Table 6. Theoretical and Experimentally Derived Spin Densities of Propargyl[a]

nucleus	ρ_e	$\Delta\rho_{vib}$	total	measured[b]
H (meth.)	−12.38	+0.31	−12.07	−12.13(2)[c]
C (meth.)	54.62	+16.60	71.22	69.47(4)[d]
C (center)	−62.59	+3.85	−58.73	−58.09(3)[d]
C (acet.)	32.22	+14.42	46.64	45.66(4)[d]
H (acet.)	−8.76	+0.66	−8.10	−8.126(5)[c]

[a]All values are given in 10^{-3} a.u. [b]The values in parentheses equal the 2-σ uncertainties in units of the last digit. [c]Ref 12. [d]This work.

https://doi.org/10.1021/jacs.3c11220
J. Am. Chem. Soc. 2024, 146, 1512−1521

Table 7. Theoretical and Experimentally Derived Spin Densities of Cyanomethyl[a]

nucleus	ρ_e	$\Delta\rho_{vib}$	total	measured[b]
H	−14.06	+0.27	−13.79	−13.340(7)[c]
C (meth.)	66.21	+19.57	85.77	79.186(9)[d]
C (nitrile)	−64.19	+0.65	−63.54	−56.684(4)[d]
N	31.02	+0.32	31.34	29.36(1)[c]

[a]All values are given in 10^{-3} a.u. [b]The values in parentheses equal the 2-σ uncertainties in units of the last digit. [c]Ref 35. [d]This work.

presented graphically alongside the ab initio spin density isosurfaces in Figure 4. The excellent agreement between the measured and calculated ground-state spin densities suggests that both the theoretical equilibrium (i.e., spin-polarization) and vibrational (i.e., orbital-following) contributions are accurate.

In propargyl, the equilibrium spin densities at the terminal C nuclei are dominated by spin-polarization by a local p_π orbital; therefore, their relative magnitude is likely a reasonable estimate of the relative atomic spin population. The calculated methylenic/acetylenic ratio is 1.7, which is somewhat greater than the value of ∼1.5 derived from the spin-polarization of their bonded H atoms.[12] The relative spin population on the central C atom cannot be so easily inferred from its equilibrium spin density because its spin-polarization contribution is dominated instead by p_π orbitals on neighboring atoms, which contribute to the spin density with a different constant of proportionality (and, indeed, sign). The analysis of the experimental spin densities is further complicated by the large and unequal vibrational orbital-following contributions to each C atom. The methylenic and acetylenic C atoms exhibit vibrational corrections of +30 and +45%, respectively, due to out-of-plane vibrations of their bonded H atoms. The central C atom has only a small vibrational contribution of a few percent because it is bonded only to other heavy atoms.

Similar effects are calculated and observed for cyanomethyl. The measured spin density for each atom is remarkably similar to that of the corresponding atoms in propargyl, except for the acetylenic C in propargyl and the N atom in cyanomethyl. The measured spin density for the former is 50% larger than that for the latter. This difference is almost entirely due to C−H vibrational corrections that are absent for the N atom. The calculated equilibrium spin densities in fact differ by only 4%, from which we can conclude that the total atomic spin populations are similar.

These issues highlight the difficulty in using isotropic HCCs alone to infer the atomic spin populations in π radicals. In contrast, the anisotropic coupling parameter, T_{aa}, provides a more selective, direct, and robust electronic probe of the π spin density. This quantity is proportional to the expectation value of $\langle[3\cos^2(\theta) - 1]/r^3\rangle$ over the unpaired electronic spin density, where r measures the distance from a given nucleus, and θ is the angle with the inertial a axis. For C and N, the anisotropic coupling parameters are sensitive to the spin population in the local atomic p orbitals because of the rapidly damped r^{-3} factor and the $[3\cos^2(\theta) - 1]$ angular factor, which is zero for s orbitals. The experimental spin anisotropies derived from the measured T_{aa} parameter for each nucleus (eq 2) are summarized in Figure 4. The ratio of the methylenic and acetylenic C atoms is 1.59, which we believe is the most robust experimental estimate of the ratio of their spin populations. In the language of resonance forms, this implies relative contributions of the idealized ethynyl methyl and allenyl limits of

$$\dot{C}H_2{-}C{\equiv}CH \;\leftrightarrow\; CH_2{=}C{=}\dot{C}H$$
$$\mathbf{61}\% \qquad\qquad \mathbf{39}\%$$

Based on an atomic partitioning of an ROHF-CCSD(T) spin density using Mulliken populations, Jochnowitz et al.[19] estimated these contributions to be 65 and 35%, respectively.

A parallel analysis can be applied to cyanomethyl. The atomic $\langle r^{-3}\rangle$ expectation values of the C and N 2p orbitals are 2.0 and 3.6 a.u., respectively. After correcting for this factor in the measured anisotropies, the ratio of their p_π spin populations is 2.18, i.e.,

$$\dot{C}H_2{-}C{\equiv}N \;\leftrightarrow\; CH_2{=}C{=}\dot{N}$$
$$\mathbf{69}\% \qquad\qquad \mathbf{31}\%$$

While the unpaired electron prefers to reside at the methylene C atom in both molecules, this asymmetry is considerably stronger in cyanomethyl. The imbalance is driven by the larger electronegativity of N vs C, presenting a simple but vivid illustration of basic resonance concepts from organic chemistry.

The unpaired spin distribution in π-conjugated radicals has a profound effect on their reactivity and thermochemistry. The structural and electronic properties derived from our spectroscopic measurements imply a preference for radical attack and recombination at the methylenic C atom in both propargyl and cyanomethyl. This conclusion is supported by a

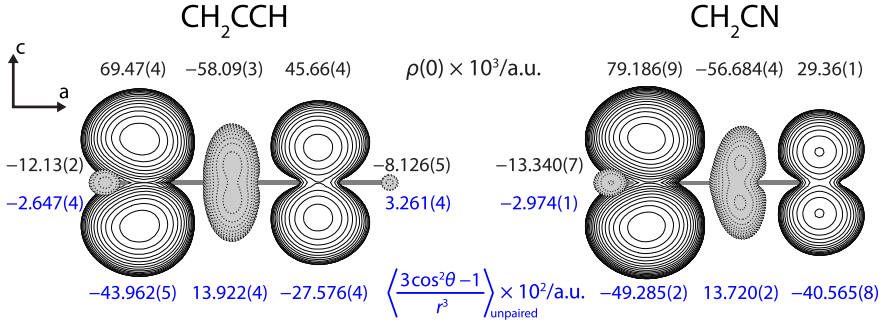

Figure 4. Electronic spin densities of propargyl and cyanomethyl. The spin density isosurface (frozen-core ROHF-CCSD(T)/cc-pVTZ) is plotted at $\rho = \pm$ 0.005 a.u. (solid contours = +, dashed contours = −). The numbers above each atom (black) are the experimentally derived vibrationally averaged spin densities at the atomic nuclei, and the numbers below (blue) are the respective spin anisotropies about the a axis. Values for the protons are derived from the normal isotopologues[12,35] and those for the carbon nuclei from the single-^{13}C isotopic species (Tables 1 and 2).

https://doi.org/10.1021/jacs.3c11220
J. Am. Chem. Soc. 2024, 146, 1512−1521

variety of experimental findings. For example, O_2 addition to propargyl in low-temperature argon matrices[71] and liquid helium droplets[72] results in exclusive formation of the propargyl peroxyl radical, $^{\bullet}OO-CH_2-C{\equiv}CH$. No $^{\bullet}OO-CH{=}C{=}CH_2$ isomer is observed because addition at the methylenic C has a very small or zero barrier while addition at the acetylenic C has a barrier of ∼3−8 kcal/mol.[72−75] The increased localization of the unpaired electron in cyanomethyl compared with propargyl is reflected in the bond dissociation energies (BDEs) of their closed-shell parents. The BDEs are $D_0(H-CH_2CN)$ = 95.18(14) kcal/mol and $D_0(H-CH_2CCH)$ = 90.21(7) kcal/mol (obtained from the Argonne Active Thermochemical Tables, ATcT[76−78]), implying a decrease of 5 kcal/mol from the CH_2CN resonance stabilization energy relative to CH_2CCH. The delocalized "bidentate" radical character of propargyl leads to three initial self-reaction adducts: head-to-head ($CH_2CCH-CHCCH_2$), tail-to-tail ($CHCCH_2-CH_2CCH$), and head-to-tail ($CH_2CCH-CH_2CCH$),[5,7] while the comparatively "monodentate" cyanomethyl can only recombine by forming a C−C bond.[79]

CONCLUSIONS

We have presented a comprehensive analysis of the molecular geometry and π-delocalized electronic structure of propargyl and cyanomethyl, two prototypical organic radicals. These properties elucidate trends in the reactivity and bond energies within their isoelectronic chemical family, showing a vivid example of the effects of changes in the relative electronegativity. It would be illuminating to extend this structural analysis to the ^{13}C and ^{17}O isotopologues of other species isoelectronic to propargyl and cyanomethyl, such as the ketenyl (OCCH)[80,81] and isocyanato (NCO) radicals.[82−85] These molecules are linear or quasilinear, with Renner−Teller-active $^2\Pi$ electronic states.[86−90] The high electronegativity of O should make $O{=}C{=}CH^{\bullet}$ and $^{\bullet}N{=}C{=}O$ the dominant resonance forms, which is a simple prediction to test with the electronic property information revealed by hyperfine analysis. Recent advances from our laboratory in the hyperfine-resolved rotational spectroscopy of aromatic[91] and organometallic[92] radicals demonstrate that exhaustive isotopic analysis has the potential to quantify the precise structural and electronic properties of even larger and more chemically diverse species. These types of studies will provide the vital physical insights needed to understand the pivotal role radicals play in the chemistry of atmospheric, combustion, and astrophysical environments.

ASSOCIATED CONTENT

Supporting Information

The Supporting Information is available free of charge at https://pubs.acs.org/doi/10.1021/jacs.3c11220.

Experimental line lists (`.lin`), Hamiltonian parameter files (`.par`, `.var`), and line-by-line fit results (`.fit`) for all nine propargyl isotopologues as well as $^{13}CH_2CN$ and $CH_2{}^{13}CN$ (ZIP)

AUTHOR INFORMATION

Corresponding Authors

P. Bryan Changala − *Center for Astrophysics|Harvard & Smithsonian, Cambridge, Massachusetts 02138, United States;* orcid.org/0000-0003-0304-9814; Email: bryan.changala@cfa.harvard.edu

Michael C. McCarthy − *Center for Astrophysics|Harvard & Smithsonian, Cambridge, Massachusetts 02138, United States;* orcid.org/0000-0001-9142-0008; Email: mccarthy@cfa.harvard.edu

Authors

Peter R. Franke − *Department of Chemistry, University of Florida, Gainesville, Florida 32611, United States*

John F. Stanton − *Department of Chemistry, University of Florida, Gainesville, Florida 32611, United States;* orcid.org/0000-0003-2345-9781

G. Barney Ellison − *Department of Chemistry, University of Colorado, Boulder, Colorado 80309, United States;* orcid.org/0000-0003-3107-1613

Complete contact information is available at: https://pubs.acs.org/10.1021/jacs.3c11220

Notes

The authors declare no competing financial interest.

ACKNOWLEDGMENTS

This work is dedicated to the memory of W. Carl Lineberger. Carl was both an outstanding person and scientist who profoundly affected the authors of this paper during his long and distinguished career. While his presence in the field will be missed by many, the far-reaching impact of his work will endure for generations of scientists. P.B.C. and M.C.M. acknowledge the support from the National Science Foundation (award no. AST-1908576). P.R.F. and J.F.S. were supported by the U.S. Department of Energy, Office of Science, Office of Basic Energy Sciences, Chemical Sciences, Geosciences, and Biosciences Division, under contract no. DE-SC0018164.

REFERENCES

(1) Frenklach, M. Reaction mechanism of soot formation in flames. *Phys. Chem. Chem. Phys.* **2002**, *4*, 2028−2037.

(2) Schmidt, T. W. The electronic spectroscopy of resonance-stabilised hydrocarbon radicals. *Int. Rev. Phys. Chem.* **2016**, *35*, 209−242.

(3) Raj, A.; Al Rashidi, M. J.; Chung, S. H.; Sarathy, S. M. PAH growth initiated by propargyl addition: Mechanism development and computational kinetics. *J. Phys. Chem. A* **2014**, *118*, 2865−2885.

(4) Miller, J. A.; Melius, C. F. Kinetic and thermodynamic issues in the formation of aromatic compounds in flames of aliphatic fuels. *Combust. Flame* **1992**, *91*, 21−39.

(5) Miller, J. A.; Klippenstein, S. J. The recombination of propargyl radicals and other reactions on a C_6H_6 potential. *J. Phys. Chem. A* **2003**, *107*, 7783−7799.

(6) Constantinidis, P.; Hirsch, F.; Fischer, I.; Dey, A.; Rijs, A. M. Products of the Propargyl Self-Reaction at High Temperatures Investigated by IR/UV Ion Dip Spectroscopy. *J. Phys. Chem. A* **2017**, *121*, 181−191.

(7) Zhao, L.; Lu, W.; Ahmed, M.; Zagidullin, M. V.; Azyazov, V. N.; Morozov, A. N.; Mebel, A. M.; Kaiser, R. I. Gas-phase synthesis of benzene via the propargyl radical self-reaction. *Sci. Adv.* **2021**, *7*, No. eabf0360.

(8) Johansson, K. O.; Head-Gordon, M. P.; Schrader, P. E.; Wilson, K. R.; Michelsen, H. A. Resonance-stabilized hydrocarbon-radical chain reactions may explain soot inception and growth. *Science* **2018**, *361*, 997−1000.

(9) Morter, C. L.; Domingo, C.; Farhat, S. K.; Cartwright, E.; Glass, G. P.; Curl, R. F. Rotationally resolved spectrum of the ν_1 CH stretch of the propargyl radical (H_2CCCH). *Chem. Phys. Lett.* **1992**, *195*, 316−321.

(10) Sumiyoshi, Y.; Imajo, T.; Tanaka, K.; Tanaka, T. Infrared diode laser spectroscopic detection of the propargyl radical produced in a supersonic jet expansion by UV laser photolysis. *Chem. Phys. Lett.* **1994**, *231*, 569−573.
(11) Tanaka, K.; Harada, T.; Sakaguchi, K.; Harada, K.; Tanaka, T. Time-resolved diode laser spectroscopy of the ν_6 band of propargyl produced by the UV photolysis of allene. *J. Chem. Phys.* **1995**, *103*, 6450−6458.
(12) Tanaka, K.; Sumiyoshi, Y.; Ohshima, Y.; Endo, Y.; Kawaguchi, K. Pulsed discharge nozzle Fourier transform microwave spectroscopy of the propargyl radical (H_2CCCH). *J. Chem. Phys.* **1997**, *107*, 2728−2733.
(13) Yuan, L.; DeSain, J.; Curl, R. Analysis of the K-Subband Structure of the ν_1 Fundamental of Propargyl Radical $H_2CC{\equiv}CH$. *J. Mol. Spectrosc.* **1998**, *187*, 102−108.
(14) Chang, C.-H.; Nesbitt, D. J. Sub-Doppler infrared spectroscopy of propargyl radical (H_2CCCH) in a slit supersonic expansion. *J. Chem. Phys.* **2015**, *142*, 244313.
(15) Kochi, J. K.; Krusic, P. J. Electron Spin Resonance of Free Radicals from Acetylenes and Allenes. *J. Am. Chem. Soc.* **1970**, *92*, 4110−4114.
(16) Kasai, P. H. Electron Spin Resonance Studies of Vinyl, Propargyl, and Butatrienyl Radicals Isolated in Argon Matrices. *J. Am. Chem. Soc.* **1972**, *94*, 5950−5956.
(17) Jacox, M. E.; Milligan, D. E. Matrix isolation study of the vacuum ultraviolet photolysis of allene and methylacetylene. Vibrational and electronic spectra of the species C_3, C_3H, C_3H_2, and C_3H_3. *Chem. Phys.* **1974**, *4*, 45−61.
(18) Huang, J. W.; Graham, W. R. M. Fourier transform infrared study of tricarbon hydride radicals trapped in Ar at 10 K. *J. Chem. Phys.* **1990**, *93*, 1583−1596.
(19) Jochnowitz, E. B.; Zhang, X.; Nimlos, M. R.; Varner, M. E.; Stanton, J. F.; Ellison, G. B. Propargyl Radical: Ab Initio Anharmonic Modes and the Polarized Infrared Absorption Spectra of Matrix-Isolated $HCCCH_2$. *J. Phys. Chem. A* **2005**, *109*, 3812−3821.
(20) Zhang, X.; Sander, S. P.; Chaimowitz, A.; Ellison, G. B.; Stanton, J. F. Detection of vibrational bending mode ν_8 and overtone bands of the propargyl radical, $HCCCH_2$ $\tilde{X}B_1$. *J. Phys. Chem. A* **2010**, *114*, 12021−12027.
(21) Fessenden, R. W.; Schuler, R. H. Electron Spin Resonance Studies of Transient Alkyl Radicals. *J. Chem. Phys.* **1963**, *39*, 2147−2195.
(22) Eckhoff, W. C.; Miller, C. E.; Billera, C. F.; Engel, P. S.; Curl, R. F. The C−D Stretch of Monodeuterated Propargyl Radical (CH_2CCD). *J. Mol. Spectrosc.* **1997**, *186*, 193−202.
(23) Schrader, D. M.; Karplus, M. Orbital Following in the Methyl Radical. *J. Chem. Phys.* **1964**, *40*, 1593−1601.
(24) Grabow, J. U.; Palmer, E. S.; McCarthy, M. C.; Thaddeus, P. Supersonic-jet cryogenic-resonator coaxially oriented beam-resonator arrangement Fourier transform microwave spectrometer. *Rev. Sci. Instrum.* **2005**, *76*, 093106.
(25) Crabtree, K. N.; Martin-Drumel, M.-A.; Brown, G. G.; Gaster, S. A.; Hall, T. M.; McCarthy, M. C. Microwave spectral taxonomy: A semi-automated combination of chirped-pulse and cavity Fourier-transform microwave spectroscopy. *J. Chem. Phys.* **2016**, *144*, 124201.
(26) Gordon, V. D.; McCarthy, M. C.; Apponi, A. J.; Thaddeus, P. Rotational Spectra of Sulfur-Carbon Chains. I. The Radicals C_4S, C_5S, C_6S, C_7S, C_8S, and C_9S. *Astrophys. J. Suppl.* **2001**, *134*, 311−317.
(27) Küpper, J.; Merritt, J. M.; Miller, R. E. Free radicals in superfluid liquid helium nanodroplets: A pyrolysis source for the production of propargyl radical. *J. Chem. Phys.* **2002**, *117*, 647−652.
(28) McCarthy, M. C.; Lee, K. L. K.; Carroll, P. B.; Porterfield, J. P.; Changala, P. B.; Thorpe, J. H.; Stanton, J. F. Exhaustive Product Analysis of Three Benzene Discharges by Microwave Spectroscopy. *J. Phys. Chem. A* **2020**, *124*, 5170−5181.
(29) Smith, P.; Kaba, R.; Smith, T.; Pearson, J.; Wood, P. EPR study of radicals formed from aliphatic nitriles. *J. Magn. Reson.* **1975**, *18*, 254−264.
(30) Saito, S.; Yamamoto, S.; Irvine, W. M.; Ziurys, L. M.; Suzuki, H.; Ohishi, M.; Kaifu, N. Laboratory detection of a new interstellar free radical $CH_2CN(^2B_1)$. *Astrophys. J.* **1988**, *334*, L113.
(31) Ahmad, I. K.; Ozeki, H.; Saito, S.; Botschwina, P. A new phosphorus bearing derivative of the methyl radical, CH_2CP, studied by microwave spectroscopy and ab initio calculation. *J. Chem. Phys.* **1998**, *109*, 4252−4257.
(32) Saito, S.; Yamamoto, S. The microwave spectrum of the cyanomethyl radical $CH_2CN(^2B_1)$. *J. Chem. Phys.* **1997**, *107*, 1732−1739.
(33) Ozeki, H.; Hirao, T.; Saito, S.; Yamamoto, S. Laboratory Microwave Spectroscopy of the Cyanomethyl Radical, CH_2CN. *Astrophys. J.* **2004**, *617*, 680−684.
(34) Vastel, C.; Yamamoto, S.; Lefloch, B.; Bachiller, R. Hyperfine structure of the cyanomethyl radical (CH_2CN) in the L1544 prestellar core. *Astron. Astrophys.* **2015**, *582*, L3.
(35) Chitarra, O.; Pirali, O.; Spaniol, J.-T.; Hearne, T. S.; Loison, J.-C.; Stanton, J. F.; Martin-Drumel, M.-A. Pure Rotational Spectroscopy of the CH_2CN Radical Extended to the Sub-Millimeter Wave Spectral Region. *J. Phys. Chem. A* **2022**, *126*, 7502−7513.
(36) Matthews, D. A.; Cheng, L.; Harding, M. E.; Lipparini, F.; Stopkowicz, S.; Jagau, T.-C.; Szalay, P. G.; Gauss, J.; Stanton, J. F. Coupled-cluster techniques for computational chemistry: The CFOUR program package. *J. Chem. Phys.* **2020**, *152*, 214108.
(37) Stanton, J. F.; Gauss, J.; Cheng, L.; Harding, M. E.; Matthews, D. A.; Szalay, P. G.; Auer, A.; Asthana, A.; Bartlett, R.; Benedikt, U. et al. *CFOUR, Coupled-Cluster Techniques for Computational Chemistry, a Quantum-Chemical Program Package*. version 2.1, 2023. available at http://www.cfour.de.
(38) Gauss, J.; Lauderdale, W. J.; Stanton, J. F.; Watts, J. D.; Bartlett, R. J. Analytic energy gradients for open-shell coupled-cluster singles and doubles (CCSD) calculations using restricted open-shell Hartree—Fock (ROHF) reference functions. *Chem. Phys. Lett.* **1991**, *182*, 207−215.
(39) Woon, D. E.; Dunning, T. H. Gaussian basis sets for use in correlated molecular calculations. V. Core-valence basis sets for boron through neon. *J. Chem. Phys.* **1995**, *103*, 4572−4585.
(40) Mills, I. M. *Molecular Spectroscopy: Modern Research*; Rao, K. N., Mathews, C. W., Eds.; Academic Press: New York, 1972; pp 115−140, Chapter 3.2.
(41) Flygare, W. H. Magnetic interactions in molecules and an analysis of molecular electronic charge distribution from magnetic parameters. *Chem. Rev.* **1974**, *74*, 653−687.
(42) Heim, Z. N.; Amberger, B. K.; Esselman, B. J.; Stanton, J. F.; Woods, R. C.; McMahon, R. J. Molecular structure determination: Equilibrium structure of pyrimidine (m-$C_4H_4N_2$) from rotational spectroscopy ($r_{e,SE}$) and high-level ab initio calculation (r_e) agree within the uncertainty of experimental measurement. *J. Chem. Phys.* **2020**, *152*, 104303.
(43) Changala, P. B. *NITROGEN*. version 2.1.2, 2021. https://github.com/bchangala/nitrogen.
(44) *Mathematica*. version 12: Champaign, IL, 2020. https://www.wolfram.com/mathematica.
(45) Kucharski, S. A.; Włoch, M.; Musiał, M.; Bartlett, R. J. Coupled-cluster theory for excited electronic states: The full equation-of-motion coupled-cluster single, double, and triple excitation method. *J. Chem. Phys.* **2001**, *115*, 8263−8266.
(46) Kállay, M.; Gauss, J. Calculation of excited-state properties using general coupled-cluster and configuration-interaction models. *J. Chem. Phys.* **2004**, *121*, 9257−9269.
(47) Almlöf, J.; Taylor, P. R. General contraction of Gaussian basis sets. I. Atomic natural orbitals for first- and second-row atoms. *J. Chem. Phys.* **1987**, *86*, 4070−4077.
(48) McCaslin, L.; Stanton, J. Calculation of fundamental frequencies for small polyatomic molecules: a comparison between correlation consistent and atomic natural orbital basis sets. *Mol. Phys.* **2013**, *111*, 1492−1496.
(49) Watts, J. D.; Gauss, J.; Bartlett, R. J. Open-shell analytical energy gradients for triple excitation many-body, coupled-cluster

https://doi.org/10.1021/jacs.3c11220
J. Am. Chem. Soc. 2024, 146, 1512−1521

methods: MBPT(4), CCSD+T(CCSD), CCSD(T),and QCISD(T). *Chem. Phys. Lett.* **1992**, *200*, 1−7.
(50) Dunning, T. H., Jr. Gaussian basis sets for use in correlated molecular calculations. I. The atoms boron through neon and hydrogen. *J. Chem. Phys.* **1989**, *90*, 1007−1023.
(51) Auer, A. A.; Gauss, J.; Stanton, J. F. Quantitative prediction of gas-phase C13 nuclear magnetic shielding constants. *J. Chem. Phys.* **2003**, *118*, 10407−10417.
(52) Jagau, T.-C.; Gauss, J.; Ruud, K. Analytic evaluation of the dipole Hessian matrix in coupled-cluster theory. *J. Chem. Phys.* **2013**, *139*, 154106.
(53) Watson, J. K. G. Determination of Centrifugal Distortion Coefficients of Asymmetric-Top Molecules. *J. Chem. Phys.* **1967**, *46*, 1935−1949.
(54) Brown, J. M.; Sears, T. J. A reduced form of the spin-rotation Hamiltonian for asymmetric-top molecules, with applications to HO_2 and NH_2. *J. Mol. Spectrosc.* **1979**, *75*, 111−133.
(55) Gordy, W.; Cook, R. L. *Microwave Molecular Spectra*, 3rd ed.; John Wiley & Sons: New York, 1984.
(56) Pickett, H. M. The fitting and prediction of vibration-rotation spectra with spin interactions. *J. Mol. Spectrosc.* **1991**, *148*, 371−377.
(57) Curl, R. F. The relationship between electron spin rotation coupling constants and *g*-tensor components. *Mol. Phys.* **1965**, *9*, 585−597.
(58) Müller, H. S. P.; Thorwirth, S.; Lewen, F. Rotational spectroscopy of singly ^{13}C substituted isotopomers of propyne and determination of a semi-empirical equilibrium structure. *J. Mol. Struct.* **2020**, *1207*, 127769.
(59) Auer, A. A.; Gauss, J. Equilibrium structure and fundamental frequencies of allene. *Phys. Chem. Chem. Phys.* **2001**, *3*, 3001−3005.
(60) Puzzarini, C.; Cazzoli, G. Equilibrium structure of methyl-cyanide. *J. Mol. Spectrosc.* **2006**, *240*, 260−264.
(61) Tamassia, F.; Cané, E.; Fusina, L.; Di Lonardo, G. The experimental equilibrium structure of acetylene. *Phys. Chem. Chem. Phys.* **2016**, *18*, 1937−1944.
(62) Craig, N. C.; Groner, P.; McKean, D. C. Equilibrium Structures for Butadiene and Ethylene: Compelling Evidence for Π-Electron Delocalization in Butadiene. *J. Phys. Chem. A* **2006**, *110*, 7461−7469.
(63) Demaison, J.; Craig, N. C.; Gurusinghe, R.; Tubergen, M. J.; Rudolph, H. D.; Coudert, L. H.; Szalay, P. G.; Császár, A. G. Fourier Transform Microwave Spectrum of Propene-3-d_1 (CH_2=$CHCH_2D$), Quadrupole Coupling Constants of Deuterium, and a Semiexperimental Equilibrium Structure of Propene. *J. Phys. Chem. A* **2017**, *121*, 3155−3166.
(64) Stone, N. J. *Table of Nuclear Magnetic Dipole and Electric Quadrupole Moments, INDC(NDS)-0658*; IAEA Nuclear Data Section: Vienna, Austria, 2014.
(65) Frosch, R. A.; Foley, H. M. Magnetic Hyperfine Structure in Diatomic Molecules. *Phys. Rev.* **1952**, *88*, 1337−1349.
(66) McConnell, H. M.; Chesnut, D. B. Theory of Isotropic Hyperfine Interactions in π-Electron Radicals. *J. Chem. Phys.* **1958**, *28*, 107−117.
(67) Fessenden, R. W. Electron spin resonance spectra of some isotopically substituted hydrocarbon radicals. *J. Phys. Chem.* **1967**, *71*, 74−83.
(68) Weltner, W. *Magnetic Atoms and Molecules*; Dover: New York, 1989.
(69) Ellinger, Y.; Pauzat, F.; Barone, V.; Douady, J.; Subra, R. Ab initio study of the vibrational dependence of hyperfine coupling constants in the methyl, silyl, and formaldehyde anion radicals. *J. Chem. Phys.* **1980**, *72*, 6390−6397.
(70) Adam, A. Y.; Yachmenev, A.; Yurchenko, S. N.; Jensen, P. Ro-vibrational averaging of the isotropic hyperfine coupling constant for the methyl radical. *J. Chem. Phys.* **2015**, *143*, 244306.
(71) Jochnowitz, E. B.; Zhang, X.; Nimlos, M. R.; Flowers, B. A.; Stanton, J. F.; Ellison, G. B. Infrared Spectrum of the Propargyl Peroxyl Radical, HCC—CH_2OO $X\sim^2A''$. *J. Phys. Chem. A* **2010**, *114*, 1498−1507.
(72) Moradi, C. P.; Morrison, A. M.; Klippenstein, S. J.; Goldsmith, C. F.; Douberly, G. E. Propargyl + O_2 Reaction in Helium Droplets: Entrance Channel Barrier or Not? *J. Phys. Chem. A* **2013**, *117*, 13626−13635.
(73) Hahn, D. K.; Klippenstein, S. J.; Miller, J. A. A theoretical analysis of the reaction between propargyl and molecular oxygen. *Faraday Discuss.* **2001**, *119*, 79−100.
(74) Pham, T. V.; Trang, H. T. T.; Nguyen, H. M. T. Temperature and Pressure-Dependent Rate Constants for the Reaction of the Propargyl Radical with Molecular Oxygen. *ACS Omega* **2022**, *7*, 33470−33481.
(75) Slagle, I. R.; Gutman, D. Kinetics of the reaction of C_3H_3 with molecular oxygen from 293−900 K. *Symp. Int. Combust.* **1988**, *21*, 875−883.
(76) Ruscic, B.; Pinzon, R. E.; Morton, M. L.; von Laszevski, G.; Bittner, S. J.; Nijsure, S. G.; Amin, K. A.; Minkoff, M.; Wagner, A. F. Introduction to Active Thermochemical Tables: Several "Key" Enthalpies of Formation Revisited. *J. Phys. Chem. A* **2004**, *108*, 9979−9997.
(77) Ruscic, B.; Pinzon, R. E.; Laszewski, G. v.; Kodeboyina, D.; Burcat, A.; Leahy, D.; Montoy, D.; Wagner, A. F. Active Thermochemical Tables: thermochemistry for the 21st century. *J. Phys.: Conf. Ser.* **2005**, *16*, 561−570.
(78) Ruscic, B.; Bross, D. H. *Active Thermochemical Tables (ATcT)*. ver 1.124; Argonne National Laboratory: Lemont, IL, 2022. ATcT.anl.gov.
(79) Korth, H. G.; Lommes, P.; Sicking, W.; Sustmann, R. Rate constants for the bimolecular self-reaction of cyano-substituted alkyl radicals in solution. *Int. J. Chem. Kinet.* **1983**, *15*, 267−279.
(80) Ohshima, Y.; Endo, Y. Determination of the Hyperfine Constants for HCCO by Pulsed-Discharge-Nozzle Fourier-Transform Microwave Spectroscopy. *J. Mol. Spectrosc.* **1993**, *159*, 458−467.
(81) Endo, Y.; Hirota, E. The submillimeter-wave spectrum of the HCCO radical. *J. Chem. Phys.* **1987**, *86*, 4319−4326.
(82) Saito, S.; Amano, T. Microwave spectrum of the NCO radical. *J. Mol. Spectrosc.* **1970**, *34*, 383−389.
(83) Amano, T.; Hirota, E. Hyperfine Interactions of the Free NCO Radical in the Δ Vibronic State (ν_2 = 1). *J. Chem. Phys.* **1972**, *57*, 5608−5610.
(84) Suzuki, T.; Saito, S.; Hirota, E. Hyperfine coupling constants of NCO in by sub-Doppler spectroscopy. *J. Mol. Spectrosc.* **1986**, *120*, 414−420.
(85) Kawaguchi, K.; Saito, S.; Hirota, E. Microwave spectroscopy of the NCO radical in the ν_2 = $0^2\Pi$, ν_2 = $1^2\Delta$, and ν_2 = $2^2\Phi$ vibronic states. *Mol. Phys.* **1985**, *55*, 341−350.
(86) Simmonett, A. C.; Stibrich, N. J.; Papas, B. N.; Schaefer, H. F.; Allen, W. D. Barrier To Linearity and Anharmonic Force Field of the Ketenyl Radical. *J. Phys. Chem. A* **2009**, *113*, 11643−11650.
(87) Szalay, P. G.; Fogarasi, G.; Nemes, L. Quantum chemical coupled cluster study of the structure and spectra of the ground and first excited states of the ketenyl radical. *Chem. Phys. Lett.* **1996**, *263*, 91−99.
(88) Jerosimić, S. V. Calculation of the magnetic hyperfine structure in the ground electronic state of HCCO. *J. Mol. Spectrosc.* **2007**, *242*, 139−149.
(89) Szalay, P. G. Ab initio coupled-cluster study of $^2\Pi$ radicals in ground and excited states: application to NCO and NCS. *J. Mol. Struct.* **1997**, *410*−*411*, 305−309.
(90) Mladenović, M.; Perić, M.; Engels, B. An ab initio study of the vibronic, spin−orbit, and magnetic hyperfine structure in the $X^2\Pi$ electronic state of NCO. *J. Chem. Phys.* **2005**, *122*, 144306.
(91) Changala, P. B.; McCarthy, M. C. Hyperfine-resolved rotational spectroscopy of phenyl radical. *J. Phys. Chem. Lett.* **2023**, *14*, 5370−5376.
(92) Changala, P. B.; Genossar-Dan, N.; Brudner, E.; Gur, T.; Baraban, J. H.; McCarthy, M. C. Structural and electronic trends of optical cycling centers in polyatomic molecules revealed by microwave spectroscopy of MgCCH, CaCCH, and SrCCH. *Proc. Natl. Acad. Sci. U.S.A.* **2023**, *120*, No. e2303586120.

https://doi.org/10.1021/jacs.3c11220
J. Am. Chem. Soc. 2024, 146, 1512−1521